Adsorption of nitrate and phosphate in an aqueous solution on composites of PVA and chitosan prepared from a *Somanniathelphusa sinensis* shell

Hieu Trung Nguyen and Ha Manh Bui

ABSTRACT

In this study, chitosan was prepared from the shell of *Somanniathelphusa sinensis*, which is a crab ubiquitous in Vietnam. The 3-level, 3-factor Box–Behnken design was applied to the preparation of chitosan to investigate effects of factors such as the HCl solution concentration, protein removal time and deacetylation time on the degree of deacetylation (%DD). Scanning electron microscopy, Fourier transform infrared spectroscopy, energy-dispersive X-ray spectroscopy and gel permeation chromatography were employed to examine the chitosan structure, as well as pH titration and antibacterial testing of the chitosan solution. Results revealed that as-p chitosan comprises specific functional groups, with almost no impurities. Its average molecular weight was ~225,000 g/mol, and %DD was ~89.7%. The chitosan/PVA composite was prepared and investigated for the adsorption of nitrate and phosphate ions in water. Experimental results revealed that the adsorption capacity of a chitosan/PVA (1:2) composite is better than that of chitosan. Accordingly, the theoretical maximum adsorption capacities of nitrate and phosphate ions on chitosan were 122.0 mg/g and 344.8 mg/g, respectively. The corresponding values on the chitosan/PVA (1:2) composite were 135.1 mg/g and 384.6 mg/g. Adsorption kinetics data at 25 °C were well fitted to the pseudo-second-order model ($R^2 > 0.998$). These results revealed that crab shell chitosan and the chitosan/PVA (1:2) composite can be used for the adsorption of nitrates and phosphates in aqueous solutions.

Key words | adsorption, chitosan composite, nitrate, phosphate, polyvinyl alcohol, *Somanniathelphusa sinensis*

Hieu Trung Nguyen
Institute of Applied Technology, Thu Dau Mot University,
06 Tran Van On Street, Phu Hoa Ward, Thu Dau Mot City,
Binh Duong Province,
Vietnam

Ha Manh Bui (corresponding author)
Department of Environmental Sciences,
Saigon University,
273 An Duong Vuong Street, District 5,
Ho Chi Minh City,
Vietnam
E-mail: *manhhakg@sgu.edu.vn*

HIGHLIGHTS

- The process of preparing chitosan from the shell of *Somanniathelphusa Sinensis* was optimized by Box-Behnken design.
- The characterization of chitosan showed that it was successfully prepared with high DD value, moderate molecular weight, good antibacterial properties and no impurities.
- Chitosan/PVA composites were prepared with uniform distribution, uniform particle size.
- Crab shell chitosan and Chitosan/PVA (1:2) composite show good adsorption capacity of nitrate and phosphate ions in aqueous solution.

GRAPHICAL ABSTRACT
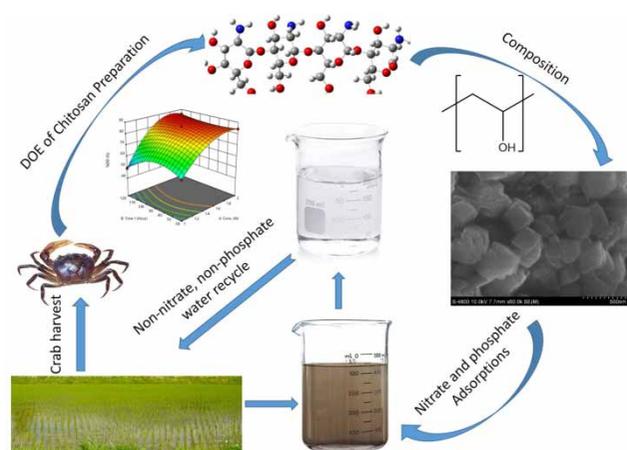
INTRODUCTION

Recently, eutrophication has become a serious problem in several rivers and lakes around the world (Bui *et al.* 2017; van Puijenbroek *et al.* 2019). Eutrophication leads to the pollution of water sources, adversely affecting the quality of water supply for drinking and human activities and increasing treatment costs for water used for aquaculture purposes and urban landscape (van Puijenbroek *et al.* 2019). This pollution is mainly related to the specific nutritional excess of nitrogen and phosphorus compounds. Two typical representative anions for the pollution of nitrogen and phosphorus are nitrate (NO_3^-) and phosphate (PO_4^{3-}), respectively. If nitrogen in water exists as nitrate, it is either completely oxidized or it persists in water. Phosphate, mainly originating from washing sources, is directly drained into sewage, causing water pollution (Dodds & Smith 2016). Several technologies have been developed to eliminate high concentrations of these two compounds, including reverse osmosis, chemical reduction, ion filtration and adsorption, with some positive results (Bhatnagar & Sillanpää 2011; Pham & Bui 2020). Chitosan and polyvinyl alcohol (PVA) have long been investigated extensively as adsorbents for removing contaminants in water, and both compounds can be used as a component in composite adsorbents. In essence, chitosan and PVA contain functional groups, including hydroxyl (PVA) and first-order amines (chitosan), with strong adsorption capacities. In an acidic environment, these groups exist as $-NH_3^+$ and $-OH_2^+$,

which strongly interact with negative ions such as NO_3^- and $H_2PO_4^-$ (Rajeswari *et al.* 2015, 2016).

Chitosan is a linear polysaccharide prepared from chitin, which is the second most abundant biopolymer on earth after cellulose. Chitosan is composed of D-glucosamine and N-acetyl-D-glucosamine units via β-$(1 \rightarrow 4)$ bonds. Chitin, chitosan and their derivatives are considered to be biologically derived polymers with bioactivity, high biological compatibility and good biodegradability; synthetic polymers do not exhibit these properties (Bonilla *et al.* 2014; Muxika *et al.* 2017). Chitosan is typically prepared using the exoskeleton of fungi and crustaceans, including krill, crayfish, jellyfish, clams, oysters and insects, as the starting materials (Srinivasan *et al.* 2018). Several studies reported the preparation of chitosan from crab shells (Sarbon *et al.* 2014; Shavandi *et al.* 2015; Rahmi *et al.* 2017; Huang *et al.* 2020); however, extremely few studies have used crab shells of *Somanniathelphusa sinensis* to prepare chitosan. Hence, chitosan is prepared using the crab shell of *S. sinensis*, which is a crab species ubiquitous in Vietnam, and chitosan/PVA composites are investigated for the adsorption of nitrate and phosphate ions in water.

Chitosan also has long been used as the major component in composite materials in several fields, including wastewater treatment (Dai *et al.* 2020; Quesada *et al.* 2020). A composite prepared from chitosan and PVA is one example (Bonilla

et al. 2014; Rajeswari et al. 2016; Das et al. 2020). However, the physical and chemical properties of this composite material considerably depend on the molecular weight and preparation conditions of each component. The decisive factor is to permit their combination in a homogeneous phase due to good compatibility of the two polymers. Stirring with heating is typically employed to prepare chitosan composites (Rajeswari et al. 2015; Rajeswari et al. 2016; Yang et al. 2020). However, such mixing does not guarantee the formation of a homogeneous phase at the microscopic level; that is, the reinforcement phase is not mixed well for uniform distribution in the matrix phase. In this study, ultrasonication was employed to support the phase dispersion process in CTS/PVA composite materials. Thus, structural properties of the resulting composite materials can be effective for the adsorption of nitrate and phosphate.

METHODS

Materials

Industrial chitosan was purchased from Safaco Inc., Vietnam. PVA ($M_w = 60,000$ g/mol) was purchased from Hi-Media, India. Analytical-reagent grade chemicals were used.

Methods

Preparation of chitosan from crab shell

Figure 1 shows the preparation process of chitosan. First, separated crab shells were boiled in water for 1 h from the moment water started to boil. Second, the crab meat was removed, and crab shells were retained. Third, crab shells were placed in an oven and dried at 80 °C for 5 h. After drying, the crab shells were cooled outdoors and finely ground using a grinder. Next, 50 g of crab shell powder was mixed with a 750 mL HCl (1.0 M, 1.5 M, 2.0 M) solution and gently stirred for 120 min at 500 rpm. The powder was separated by vacuum filtration and washed with distilled water until the pH of the filtered water was ~7.0. The powder was further mixed with a 750 mL solution of 3 M NaOH and gently stirred for (60, 90, 120) min without heating, followed by filtration and washing as described above. The raw chitin powder was mixed with acetone in a ratio of 1:15 (g/mL) and gently stirred for 20 min at room temperature. Next, the powder was filtered under vacuum and thinly dried in an oven at 70 °C for 24 h. Chitin and a 50% NaOH solution were mixed in a ratio of 1:15 (g/mL) in a 1-L flask with two necks equipped with a condenser tube and thermometer, respectively, magnetically stirred
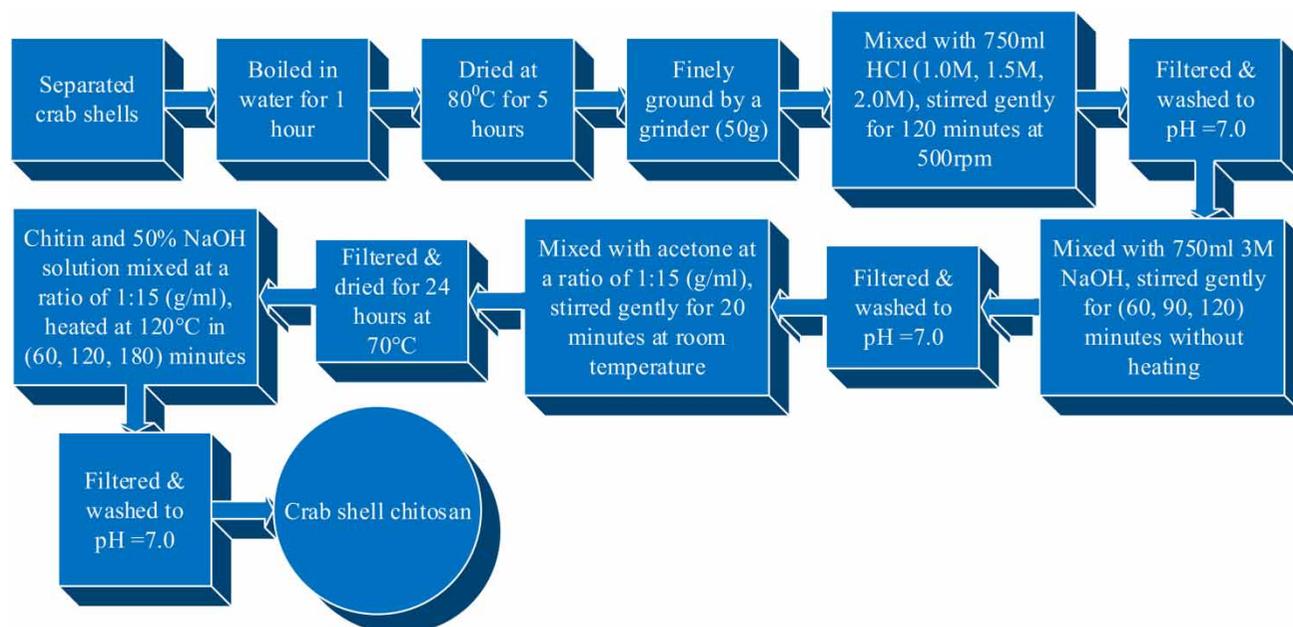

Figure 1 | Flowchart for the preparation of crab shell chitosan.

and heated at 120 °C for (60, 120, 180) min. Then, the solid was filtered, washed with distilled water until the pH was 7.0 and dried at 70 °C for 24 h. Chitin and chitosan were analysed by Fourier transform infrared (FTIR) spectroscopy, energy-dispersive X-ray spectroscopy (EDX) and gel permeation chromatography (GPC). The antibacterial activity of the chitosan solution against *Staphylococcus aureus* and *Escherichia coli* was investigated. The film of this as-prepared chitosan was analysed by scanning electron microscopy (SEM).

Determination of %DD of chitosan

Degree of deacetylation (%DD) of chitosan was calculated according to the previous method (dos Santos *et al.* 2009; Yuan *et al.* 2011; Pérez-Álvarez *et al.* 2018), which is briefly described below.

First, 0.20 g of chitosan was dissolved in 25 mL of a 0.1 M HCl solution, and distilled water was then added to obtain a 100-mL solution. Second, 0.56 g of KCl was added to the solution, stirred and gently heated until the solid was completely dissolved. Third, the solution was cooled to room temperature with stirring. Next, the pH probe was placed into the solution, and a 0.1 M NaOH solution was slowly added into the solution to adjust the solution pH to 2.0. Next, about 0.5 mL of a 0.1 M NaOH solution was used each time for titration, and the solution pH was recorded. The above procedure was repeated until the solution pH was ~11.5. The experiment was conducted in triplicate.

Preparation of Chitosan/PVA (CTS/PVA) composites

First, a PVA pellet (CTS:PVA mass ratios: 1:1, 1:2, 2:1) was added to 150 mL of distilled water. Second, the mixture was magnetically stirred and subjected to ultrasonication for 1 h using a device with a power of 500 W and a frequency of 20 KHz until PVA was completely dissolved. Next, 0.5 g of $CaCO_3$ was added to the stirred solution with simultaneous ultrasonication of the solution. Next, chitosan was added to the solution until it was mixed well. Then, a 5 M HCl solution was slowly added to the mixture with the simultaneous stirring of the mixture and ultrasonic treatment. Finally, the mixture was thinly coated into Poly(methyl methacrylate) plastic moulds and dried at

70 °C for 24 h. The obtained materials were used as adsorbents for the removal of nitrate and phosphate.

Measurement of nitrate ion adsorption capacity

The adsorbents used for nitrate adsorption experiments include industrial chitosan (Safaco CTS), crab shell chitosan (crab shell CTS) and CTS/PVA composites in three ratios of 1:1, 1:2 and 2:1, respectively. The nitrate solution used for the adsorption test exhibited a volume of 25 mL mixed with a specific concentration of NO_3^- (mg/L). The adsorbent and nitrate solution were contained in a 100-mL Erlenmeyer flask and shaken by a mechanical shaker at 200 rpm at room temperature at a given time. After shaking, the solid portion was filtered from the solution using a filter paper. Then, 10 mL of the above solution and 1 mL of a sodium salicylate solution (0.5 g of sodium salicylate in 100 mL of water) were added to a 50-mL beaker and heated at 105 °C until drying, followed by cooling the solution to room temperature. Then, 1 mL of concentrated sulfuric acid was added to the above beaker and shaken to dissolve the solid, followed by standing for 10 min. Next, 8 mL of distilled water was added and cooled, followed by the addition of 7 mL of a 30% NaOH solution. The solution was analysed for light absorption at 420 nm using a UV–Vis Jasco V-770 instrument.

Measurement of phosphate ion adsorption capacity

The experimental procedure for phosphate adsorption was similar to that of nitrate, but the difference was that the concentration of the phosphate solution was calculated as the number of mg of $H_2PO_4^-$ in 1 L of water. 10 ml of phosphate solution after filtration of solid adsorbent was added to 100 ml Erlenmeyer flask with one drop of phenolphthalein indicator solution. If the mixture was pink, the H_2SO_4 5N solution was slowly dripped into the mix and swirled until the pink color disappears. 5 ml of the reagent solution was added and the mixture was mixed and allowed to stand for 10 minutes; then the absorbance was measured using UV-Vis Jasco V-770 at a wavelength of 880 nm.

Preparation of reagent solution: 50 ml of 4N H_2SO_4 solution, 5 ml of potassium antimonyl tatrate solution (1,3715 g of $K(SbO)C_4H_4O_6.1/2H_2O$ to 500 ml with water), 15 ml of ammonium solution molybdate (20 g of

$(NH_4)_6Mo_7O_{24}.4H_2O$ in 500 ml of water) and 30 ml of ascorbic acid solution (0.176 g of ascorbic acid in 100 ml of water) were mixed in an Erlenmeyer flask of 250 ml in the same order as above. The Erlenmeyer flask was shaken steadily after each new solution was added. If the solution was cloudy during mixing, it was shaken and allowed to stand for a few minutes to clear; then, another solution was added. The reagent solution is stable for 4 hours.

RESULTS AND DISCUSSION

Optimization of preparation of crab shell chitosan

The Box–Behnken design is a high-order response surface design used for experimental optimization with fewer runs, and it does not contain an embedded factorial or a fractional factorial design (Rao & Kumar 2012). The few vital factors and its empirical ranges were investigated (Table 1) by screening designs reported in previous studies (Sarbon et al. 2014; Shavandi et al. 2015; Rahmi et al. 2017; Srinivasan et al. 2018; Huang et al. 2020). Table 2 lists the analysis of variance (ANOVA) results of %DD for chitosan.

Table 1 | Box–Behnken experimental design for the optimization of chitosan preparation

Std	Run	Factor 1 A: Conc. (M)	Factor 2 B: Time 1 (Min.)	Factor 3 C: Time 2 (Min.)	Response 1 %DD (%)
1	6	1	60	120	58.1
2	11	2	60	120	84.3
3	15	1	120	120	49.0
4	9	2	120	120	85.7
5	2	1	90	60	46.7
6	8	2	90	60	85.2
7	10	1	90	180	85.8
8	14	2	90	180	85.6
9	5	1.5	60	60	81.5
10	13	1.5	120	60	81.7
11	12	1.5	60	180	84.3
12	7	1.5	120	180	88.2
13	1	1.5	90	120	85.1
14	3	1.5	90	120	85.5
15	4	1.5	90	120	86.0

Type III-partial sum of squares was observed. A model F-value of 1,158.02 indicated that the model is significant. There was only a 0.09% chance that such a high F-value can occur due to noise. P-values less than 0.0500 indicated that model terms are significant. In this case, A, B, C, AB, AC, A^2, B^2, C^2, A^2B, A^2C and AB^2 are significant model terms. Values greater than 0.1000 indicated that model terms are not significant.

The final equation in terms of actual factors with an R^2 of 0.9999 was expressed as follows:

$$
\begin{aligned}
\%DD = {}& -338.53333 + 373.95000A + 3.33083B \\
& + 1.44403C - 1.10500AB - 1.83250AC \\
& + 0.000514BC - 73.71667A^2 - 0.025032B^2 \\
& + 0.000686C^2 - 0.393333A^2B + 0.503333A^2C \\
& + 0.013667AB^2
\end{aligned}
$$

Point prediction for chitosan synthesis conditions at A = 1.62 M, B = 95.64 min and C = 177.31 min was %DD of 90.1697, with a standard deviation of 0.450925. These conditions were applied to the preparation of chitosan with triplicate repeatability (Figure 2), and the characterization of chitosan was discussed in the following sections.

Table 2 | ANOVA for reduced cubic model

Source	Sum of Squares	df	Mean Square	F-value	p-value
Model	2,825.56	12	235.46	1,158.02	0.0009
A-Conc.	366.72	1	366.72	1,803.55	0.0006
B-Time 1	4.20	1	4.20	20.67	0.0451
C-Time 2	21.62	1	21.62	106.34	0.0093
AB	27.56	1	27.56	135.55	0.0073
AC	374.42	1	374.42	1,841.42	0.0005
BC	3.42	1	3.42	16.83	0.0546
A²	547.69	1	547.69	2,693.55	0.0004
B²	61.44	1	61.44	302.16	0.0033
C²	22.54	1	22.54	110.86	0.0089
A²B	17.40	1	17.40	85.60	0.0115
A²C	114.01	1	114.01	560.68	0.0018
AB²	75.64	1	75.64	372.02	0.0027
Pure Error	0.4067	2	0.2033		
Cor Total	2,825.96	14			

corresponded to the N–H and O–H stretching vibrational frequencies and intermolecular hydrogen bonding. In the FTIR spectrum of crab shell chitin, two peaks at 1,661 and 1,627 cm^{-1} corresponded to the stretching vibration of amide I, respectively; the former and latter peaks were assigned to the stretching vibration of $C = O$ linked with the N–H group of the inner chain via hydrogen bonding and to the hydrogen bond between $C = O$ and the hydroxymethyl group of the next unit of the same molecule, respectively. Absorption peaks at 1,557 and 1,316 cm^{-1} corresponded to the N–H bending vibration of amide II and C–N stretching vibration of amide III, respectively. In the FTIR spectrum of chitosan, the peak at 1,557 cm^{-1} was no longer observed, and a new peak at 1,596 cm^{-1} (crab shell chitosan) or 1,584 cm^{-1} (Safaco chitosan) corresponding to the NH_2 bending vibration was observed. However, a low-intensity peak corresponding to the N-H bending vibration of amide II was observed at 1,548 cm^{-1} in the FTIR spectrum of Safaco chitosan (Table 3). This result indicated that the reduction of crab shell chitin to produce chitosan is better than that of Safaco chitosan.

Figure 2 │ %DD value versus A and B factors at a deacetylation time of 120 min.

Chitosan characterization

Fourier transform infrared (FTIR) spectroscopy

FTIR spectra of chitin and chitosan samples extracted from *S. sinensis* shells were recorded and compared with that of Safaco chitosan (Figure 3). Peaks observed at 3,447 cm^{-1} for chitin samples, 3,433 cm^{-1} for extracted chitosan samples and 3,436 cm^{-1} for Safaco chitosan samples

Degree of deacetylation (DD)

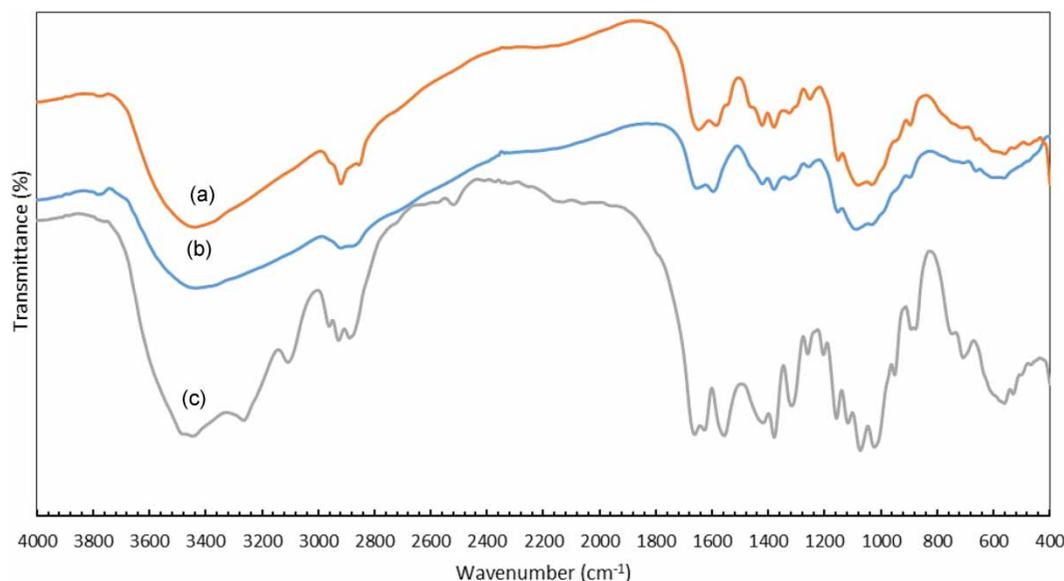The degree of deacetylation for chitosan was determined by acid–base titration using a 0.1 M NaOH standard solution

Figure 3 │ FT-IR spectra of Safaco chitosan (a), crab shell chitosan (b) and crab shell chitin (c).

Table 3 │ Typical FT-IR peaks of crab shell chitin, crab shell chitosan, Safaco chitosan

Sample	Wavenumber (cm^{-1})											
Crab shell chitin	3,447	2,928	1,661	1,557	1,417	1,380	1,316	1,158	1,117	1,073	1,024	893	709
Crab shell chitosan	3,433	2,921	1,656	1,596	1,421	1,380	1,324	1,153	–	1,089	1,034	898	663
Safaco chitosan	3,436	2,920	1,648	1,584	1,422	1,380	1,324	1,151	–	1,080	1,032	896	662
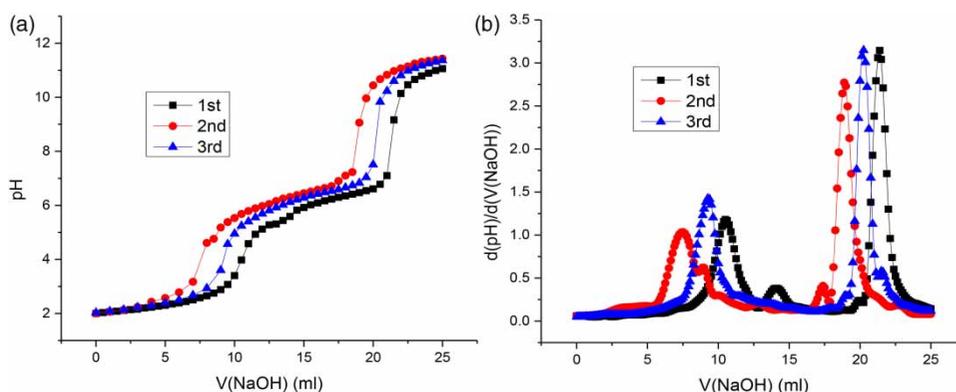
Figure 4 │ Determination method for %DD of crab shell chitosan from pH titration: (a) pH titration curves, and (b) first-order derivatives of pH titration curves.

using a pH meter. With the increase in the pH to 5.5, chitosan started to precipitate; hence, caution must be exerted for the titration of heterogeneous media. The pH was a function of the volume of the added 0.1 M NaOH solution. Two distinct equivalence points were observed in the curve of pH versus the NaOH solution volume (Figure 4(a) and Table 4). The first equivalence point corresponded to the neutralization of excess HCl used to dissolve chitosan with the NaOH solution. The second equivalence point corresponded to the neutralization reaction of the $-NH_3^+$ group on chitosan after dissolving in HCl using the added NaOH solution. The 0.1 M NaOH solution volume used at the two equivalent points was calculated by finding the maximum of the first derivative curve of pH versus the

variation in the NaOH solution volume (Figure 4(b)). %DD was calculated by the following formula (Pérez-Álvarez *et al.* 2018):

$$\%DD = \frac{(y-x).10^{-3}.M}{(y-x).10^{-3}.M + \dfrac{[w - ((y-x).10^{-3}.M.161.16)]}{203.19}}.100$$

where, y and x are the second and first equivalence, respectively (mL), M is the NaOH standard solution concentration (mol/L) and w is the mass of chitosan used for titration (g).

Determination method for the degree of deacetylation by pH titration is accurate and easily accomplished. %DD of crab shell chitosan was determined to be 89.7% ± 2.0% by this method. This value was in good agreement with the point prediction value in the Box–Behnken experimental design (90.1697%).

Gel permeation chromatography profile of chitosan

In the GPC profile of crab shell chitosan, two peaks were observed at 6.785 min (peak 1) and 10.092 min (peak 2), respectively (Figure 5). Peak 1 corresponded to the higher-
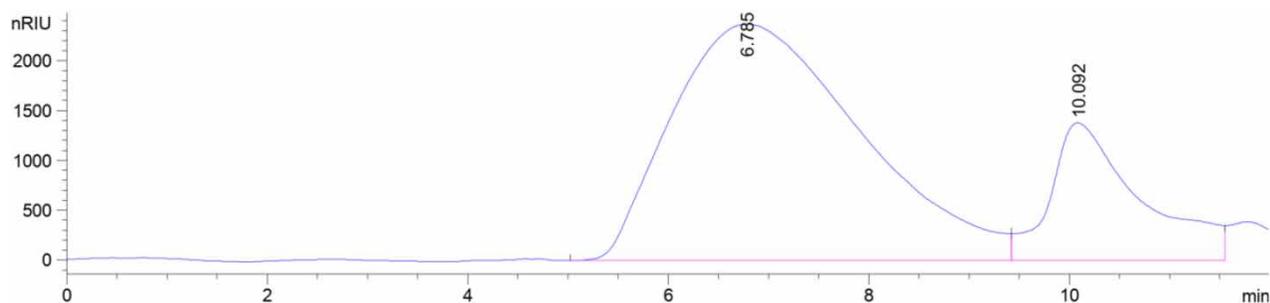
Table 4 │ Volume of the 0.1 M NaOH solution at the two equivalent points of the pH titration curve

No.	V$_{1max}$ (mL)	V$_{2max}$ (mL)	%DD (%)
1	10,49762	21,3868	87,9
2	7,51388	18,88878	91,9
3	9,25852	20,25674	89,2
%DD$_{average}$ (%)	89,7 ± 2,0		

Figure 5 │ GPC of crab shell chitosan.

molecular-weight substance, which would leave the column the earliest, and the lower-molecular weight (peak 2) would exit the column later. The results showed that the average molecular weight of peak 1 is $M_w = 225,000$ g/mol and that the dispersity of chitosan is $D = 11.63$ (Table 5). Therefore, the molecular weight of chitosan is at an average level according to the classification (100,000–300,000 g/mol). In addition, the GPC diagram also revealed that peak 2 corresponds to the substance with an average molecular weight of ~19,519 g/mol. As GPC does not allow the quantification of

the content of each peak, and according to the synthesis process, peak 2 is concluded to correspond to low-molecular-weight impurities, which can be ethanol, acetone, or glucosamine used in the preparation.

Energy-dispersive X-ray analysis of chitosan

EDX spectra of crab shell chitosan and Safaco chitosan revealed considerably different elemental compositions for the two samples (Figure 6). Safaco chitosan contained several minerals of metals such as Ca, Mg, Al and Si due to the incomplete demineralization stage. In contrast, crab shell chitosan exhibited only two main peaks of O and C, respectively (Table 6). In addition, the EDX spectrum cannot quantify elements such as H and N; hence, crab shell chitosan does not contain these two elements. This result indicated that crab shell chitosan almost no longer comprises inorganic mineral content.

Table 5 │ Average molecular weights of crab shell chitosan

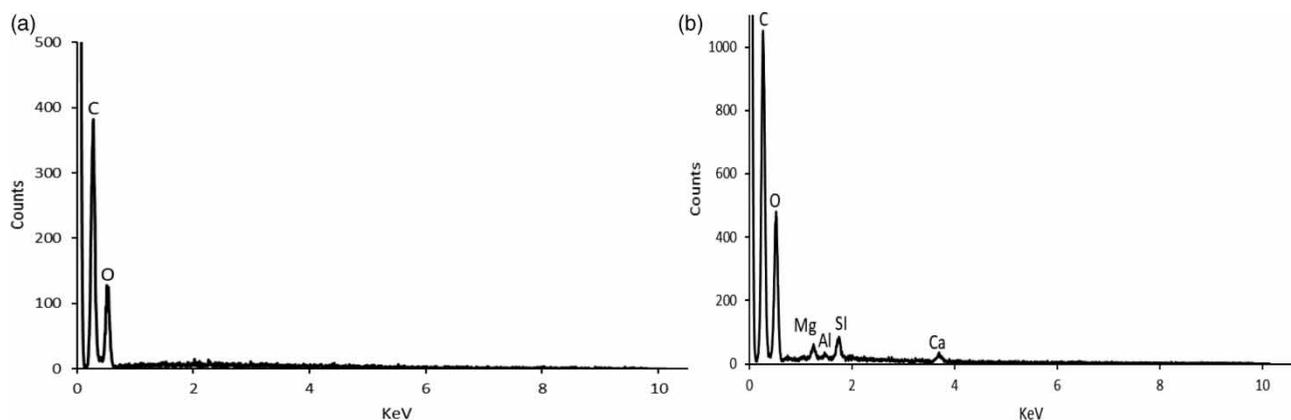|	Peak 1	Peak 2
Time (min.)	6.785	10.092
M_n (g/mol)	1.9352×10^4	11.723
M_w (g/mol)	2.2496×10^5	19.519
M_z (g/mol)	6.6028×10^5	28.546
M_v (g/mol)	2.2496×10^5	19.519

Figure 6 │ EDX spectra of (a) crab shell chitosan and (b) Safaco chitosan.

Table 6 │ Weight and atomic percentage values for elements in crab shell chitosan and Safaco chitosan

Element	Safaco chitosan		Crab shell chitosan	
	% Mass	**% Element**	**% Mass**	**% Element**
C	53.37	61.19	49.57	56.70
O	43.25	37.22	50.43	43.30
Mg	0.87	0.49	–	–
Al	0.22	0.11	–	–
Si	1.38	0.68	–	–
Ca	0.91	0.31	–	–

Scanning electron microscopy (SEM) of the chitosan film and chitosan/PVA composite

In the SEM image (Figure 7(a)) of the crab shell chitosan film, chitosan polymer molecules were agglomerated into particles, with a uniform size distribution of 50–70 nm. Meanwhile, in the SEM image of the CTS/PVA (1:2) composite sample, these two components had mixed to form square layers with a width of 100–200 nm and a thickness of 20–30 nm (Figure 7(b)). This result revealed that the composite sample is successfully prepared and that a homogeneous uniform phase is formed.

Antibacterial properties of chitosan

The antibacterial test results for the 2% chitosan solution (Figure 8) revealed that all of these samples are resistant to *S. aureus* and *E. coli*. Compared to the 2% crab shell chitosan solution (9.00 mm), the 2% solution of Safaco chitosan
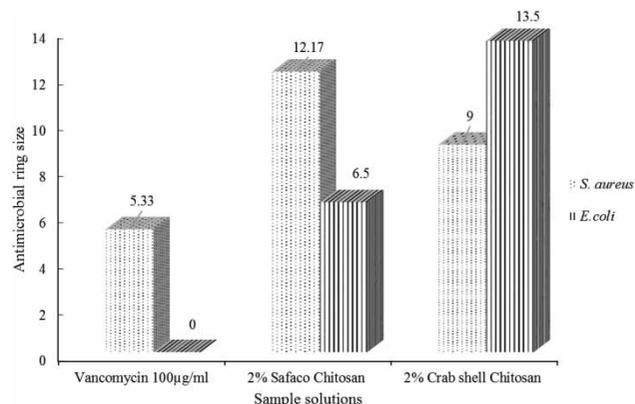
Figure 8 │ Antimicrobial Inhibition ring size of the tested samples.

was more resistant to *S. aureus* (12.17 mm); however, these two samples exhibited opposite antibacterial activities against *E. coli*: the 2% solution of crab shell chitosan was more robust (13.50 mm) than Safaco chitosan (6.50 mm). Therefore, the antibacterial effect of crab shell chitosan against *E. coli* is better than that against *S. aureus*, but the opposite result is noted for Safaco chitosan. Besides, the lowest resistance to a 100 μg/mL solution of vancomycin of these two bacteria was observed. An antibacterial effect against *E. coli* was not observed.

Adsorption of nitrate and phosphate ions

Calibration curve for determining nitrate and phosphate solution concentrations

The determination method for the nitrate or phosphate concentration involved the light absorbance measurement
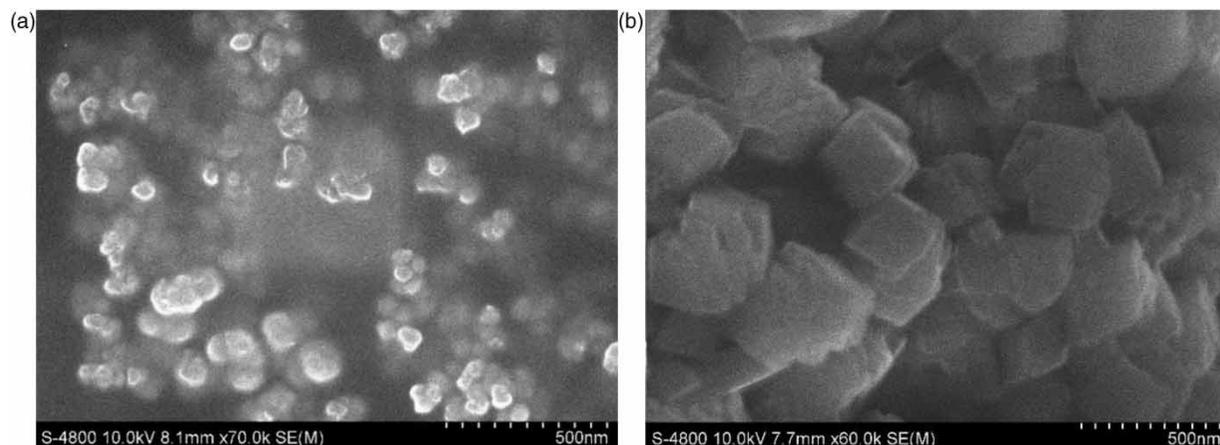
Figure 7 │ SEM images of (a) film of crab shell chitosan (b) CTS/PVA 1:2 composite.

at 880 nm (for phosphate solution) or 420 nm (for nitrate solution). Hence, a calibration curve for the absorbance versus the nitrate or phosphate solution concentration is first plotted. The calibration curve for the phosphate concentration was $ABS_1 = 0.1378Conc._1 + 0.125$ ($R_1^2 = 0.9986$), with a concentration range between 1 and 5 mg $H_2PO_4^-$/L. Meanwhile, the calibration curve for the nitrate concentration was $ABS_2 = 0.1337Conc._2 + 0.0312$ ($R_2^2 = 0.9984$), with concentrations ranging between 0.8 and 5 mg NO_3^-/L.

Effect of adsorbent dosage on the removal percentage

The adsorption of phosphate and nitrate ions was investigated by varying the adsorbent dosage (20, 50, 100, 150, 200 mg) while maintaining the other factors constant; that is, an adsorbate concentration of 5 mg/L, a solution pH of 3 before adsorption and a contact time of 120 min. With the increase in the adsorbent dosage, the removal percentage of phosphate and nitrate ions markedly increased, which was reasonable due to the increase in the number of active sites with the increase in the content (Figure 9). However, for Safaco chitosan samples, the opposite results were obtained. The opposite results can be explained by the fact that in Safaco chitosan, some phosphorus-containing mineral components are still present, and in an acidic environment, these components are dissolved the solution. Experimental results revealed that crab shell chitosan and the CTS/PVA (1:2) composite are the two best adsorbents.

Effect of pH of nitrate and phosphate solutions on the removal percentage

In this adsorption experiment, the adsorbate solution pH before adsorption was varied (3, 4, 5, 6, 7, 8) while simultaneously maintaining other factors constant; that is, an adsorbent dosage of 50 mg, an adsorbate concentration of 5 mg/L and a contact time of 120 min. Generally, the highest adsorption efficiencies for phosphate and nitrate ions were observed at pH 3; then, the adsorption efficiencies rapidly decreased with the decrease in the pH to 4 or 5, after which the efficiencies were almost unchanged (Figure 10). This result can be explained as follows: in an acidic environment, the first amino group on chitosan was protonated, and it was converted into -NH_3^+; this group exhibited strong electrostatic interactions with phosphate and nitrate anions; hence, the adsorption efficiency increases. The highest adsorption efficiency was observed for crab shell chitosan and the CTS/PVA (1:2) composite.

Effect of contact times on the removal percentage

In the experiment, the contact time was varied (10, 20, 50, 90, 120, 180 min, Figure 11) while maintaining other factors constant; that is, an adsorbent dosage of 50 mg, an adsorbate solution concentration of 5 mg/L and adsorbate solution pH of 3 before adsorption. With the increase in the contact time, the adsorption efficiencies rapidly increased after 20 min and then slowly increased with the
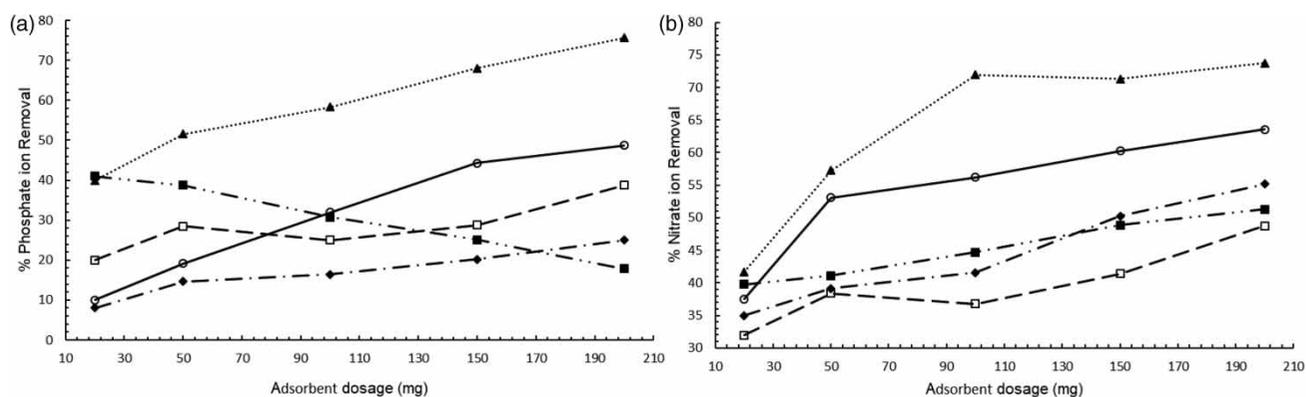

Figure 9 │ Adsorption efficiency of chitosan and composite samples at different adsorbent doses for phosphate (a) and nitrate (b) ions (■: Safaco CTS, ○: Crab shell CTS, ◆: CTS/PVA 2:1, ▲: CTS/PVA 1:2, □: CTS/PVA 1:1).
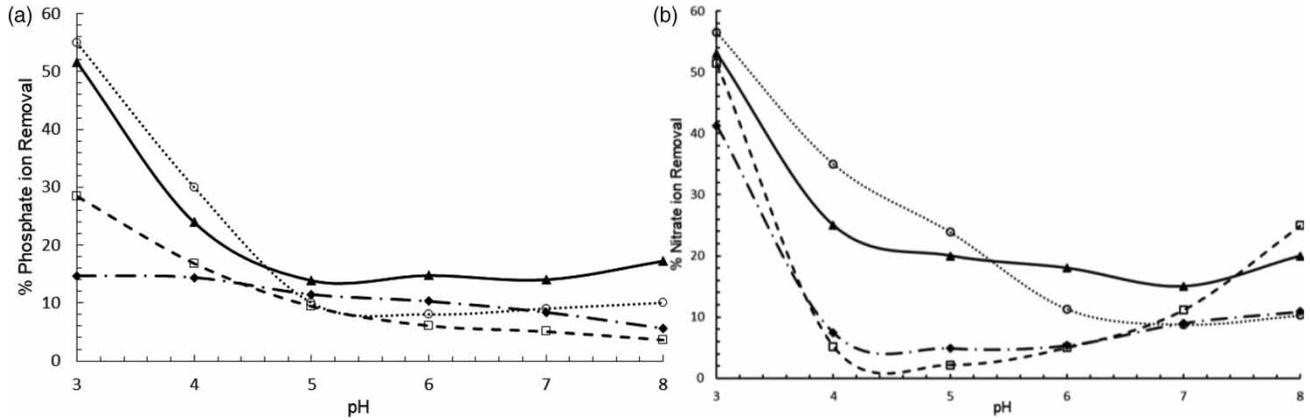
Figure 10 | Adsorption efficiencies of chitosan and composite samples at different pH values of pre-adsorption solutions for phosphate ion (a) and nitrate ion (b) (○: Crab shell CTS, ◆: CTS/PVA 2:1, ▲: CTS/PVA 1:2, □: CTS/PVA 1:1).
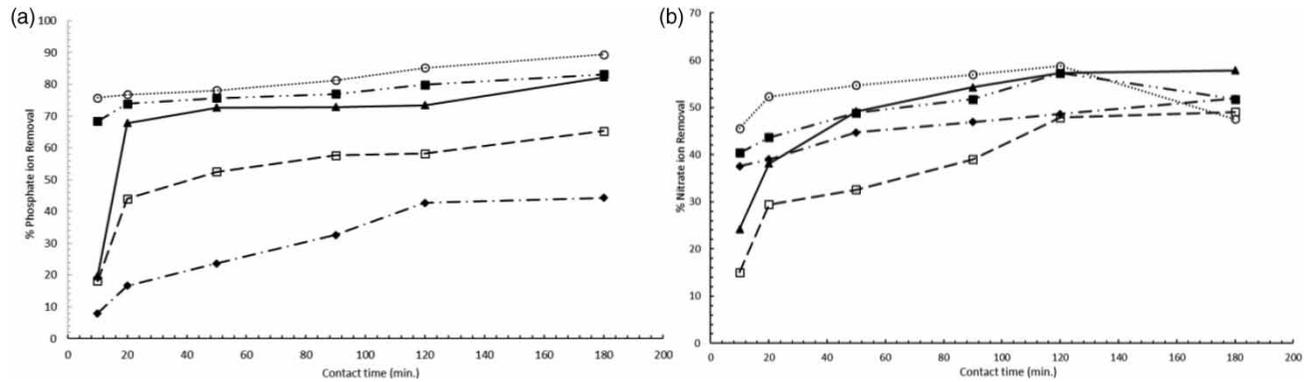

Figure 11 | Adsorption efficiency of chitosan and composite samples at different contact times for phosphate (a) and nitrate ions (b) (■: Safaco CTS, ○: Crab shell CTS, ◆: CTS/PVA 2:1, ▲: CTS/PVA 1:2, □: CTS/PVA 1:1).

contact time, and the adsorption equilibrium was established after about 120 min.

Adsorption isotherm model

To better understand the types of chemical and physical adsorption, the Langmuir and Freundlich equations were applied. The Langmuir adsorption isotherm model can be expressed as follows:

$$\frac{1}{q_e} = \frac{1}{q_{max}} + \frac{1}{bq_{max}C_e}$$

where, C_e is the equilibrium concentration of the adsorbate solution (mg/L), q_{max} is the theoretical maximum adsorption capacity (mg/g) and b is the Langmuir equilibrium constant (L/mg).

The Freundlich adsorption isotherm model can be expressed as follows:

$$\ln q_e = \ln k_f + \frac{1}{n}\ln C_e,$$

where k_f and n are the Freundlich constants.

For Langmuir isotherms, when C_e/q_e is plotted versus C_e, a straight line with a slope of $1/q_{max}$ is obtained, and q_{max} can be determined from the slope. For the Freundlich isotherms, when $\ln q_e$ is plotted with $\ln C_e$, a straight line with a slope of $1/n$ is obtained, and n can be calculated from the slope. The compatibility of experimental results with a specific model was determined by the R^2 value. The Langmuir isotherm model was more suitable for the adsorption of phosphate and nitrate over crab shell chitosan and the CTS/PVA (1:2) composite (Figures 12 and 13). The
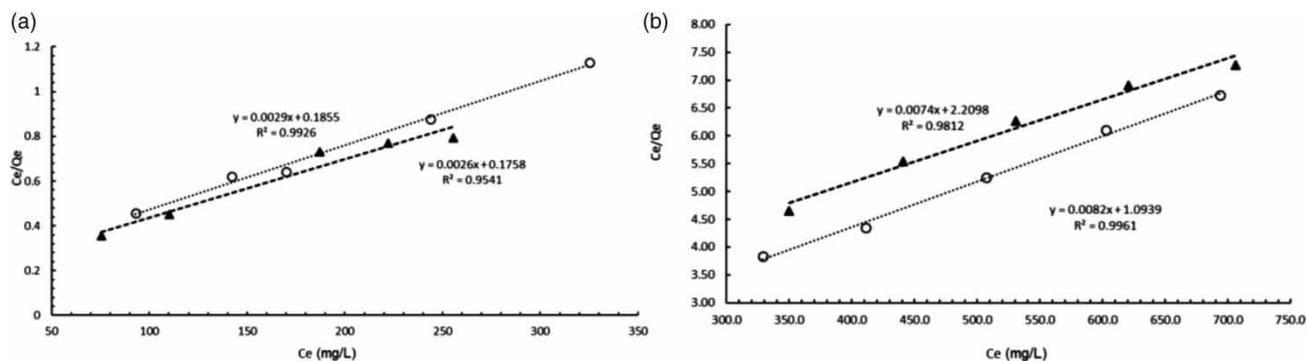
Figure 12 │ Langmuir adsorption isotherms of crab shell chitosan (◯) and CTS/PVA (1:2) (▲) for phosphate (a) and nitrate (b) ions.
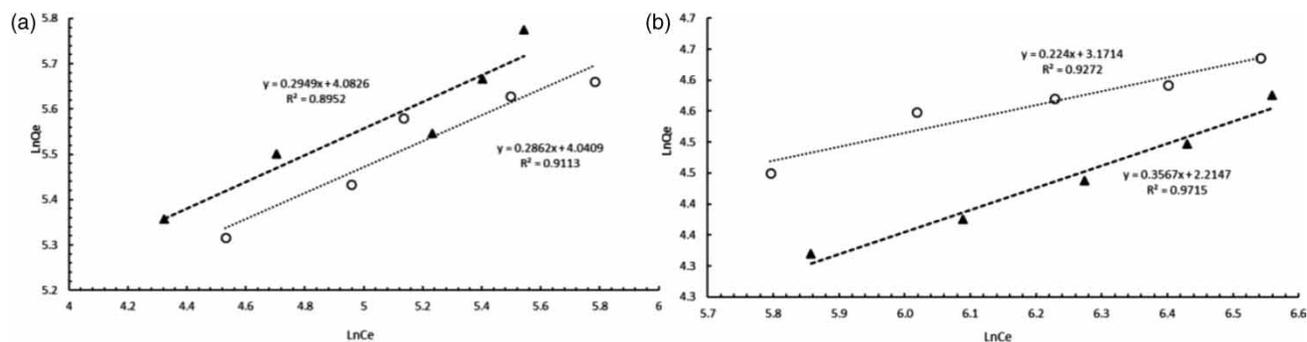

Figure 13 │ Freundlich adsorption isotherms of crab shell chitosan (◯) and CTS/PVA (1:2) (▲) for phosphate (a) and nitrate (b) ions.

q_{max} values for the adsorption of phosphate and nitrate over chitosan were 344.8 and 122.0 mg/g, respectively. The corresponding values over the CTS/PVA (1:2) composite adsorbent were 384.6 and 135.1 mg/g.

Table 7 below summarizes the adsorption efficiencies for nitrate and phosphate reported recently. In addition to the CTS/PVA composite, similar to that used herein, several other adsorbents were utilized. The comparison of adsorption capacities for nitrate and phosphate in this study with the references revealed that good results were obtained. Specifically, the nitrate adsorption capacity observed in this study was only less than that of the anionic bio-graphene nanosheet (Ghadiri *et al.* 2017), but the highest phosphate adsorption capacity was observed in this study.

Adsorption kinetic models

In this adsorption kinetic study, experiments were conducted under conditions of an adsorbent dosage of 50 mg, an adsorbate solution volume of 25 mL, an adsorbate solution concentration of 5 mg/L, a pH of 3 and a

temperature of 25 °C. Figure 13 shows the linear fitting for the pseudo-first-order (PFO) (Figure 14(a)) and pseudo-second-order (PSO) (Figure 14(b)) adsorption kinetics. The results revealed that the adsorption of nitrate and phosphate ions on crab shell CTS and the CTS/PVA (1:2) composite is best fitted to the PSO kinetics ($R^2 > 0.998$). Compared to the PSO adsorption model, the PFO adsorption kinetic model was less consistent with the experimental results, which was demonstrated by the squared correlation coefficients (R^2) for the PFO model as 0.972 and 0.717 (crab shell CTS) and 0.957 and 0.925 (CTS/PVA (1:2) composite). Accordingly, these kinetic adsorption experiments were performed at low adsorbate concentrations and followed the PSO model; hence, the mechanism of this adsorption process is confirmed to be monolayer chemical adsorption (Yang *et al.* 2020).

Desorption and regeneration of the adsorbent

For the application of adsorption to water treatment, besides the adsorption capacity of the adsorbent, reusability also

Table 7 │ Comparison of adsorption capacities of crab shell CTS and the CTS:PVA (1:2) composite for nitrate and phosphate ions

Adsorbent	Nitrate adsorption capacity (mg/g)	Phosphate adsorption capacity (mg/g)	References
Polyethylene glycol/chitosan	50.68	74.85	Rajeswari et al. (2015, 2016)
PVA/chitosan	35.03	46.19	
Al-modified biochar	89.58	57.49	Yin et al. (2018)
Magnetic cationic hydrogel	95.88	–	Li et al. (2020a)
Quaternized chitosan-zeolite-glutaraldehyde beads	62.23	–	He et al. (2020)
Anionic bio-graphene nanosheet	182.51	–	Ghadiri et al. (2017)
Mg and Al modified biochars	–	153.40	Zheng et al. (2020)
Chitosan/Fe^{3+}	–	48.6	Zhang et al. (2018)
Crosslinked chitosan/Fe^{3+}	–	31.6	
Lanthanum-coated biochar	–	93.91	Li et al. (2020b)
Crab shell CTS	122.0	344.8	This work
CTS/PVA (1:2) composite	135.1	384.6	This work
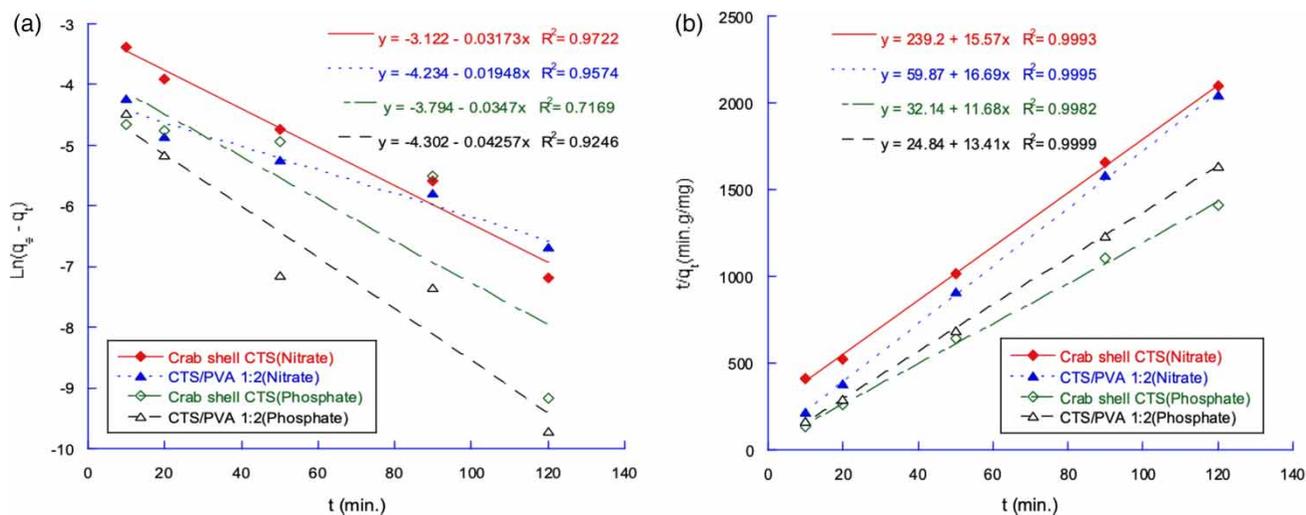
Figure 14 │ Adsorption kinetics of nitrate and phosphate ions on crab shell CTS and the CTS:PVA (1:2) composite: (a) PFO model, and (b) PSO model.

plays an equally important role. The ability of the adsorbent to be reused several times without significant reduction in efficiency reduces treatment costs, especially for high-cost adsorbents. Several factors affect the effectiveness of desorption, but binding strength appears to be the most important factor (Yang et al. 2020). In this study, nitrate and phosphate anions are adsorbed on chitosan composites via electrostatic interactions between these anions

and the protonated amino group of chitosan in an acidic medium. Therefore, when NaOH is used as a desorbent, it can completely or partially neutralize the -NH_3^+ groups, nullifying the interactions between the composite and these anions. Hence, desorption occurs almost completely. In the adsorption–desorption experiment (Figure 15), the adsorption efficiency after six cycles remained mostly unchanged.
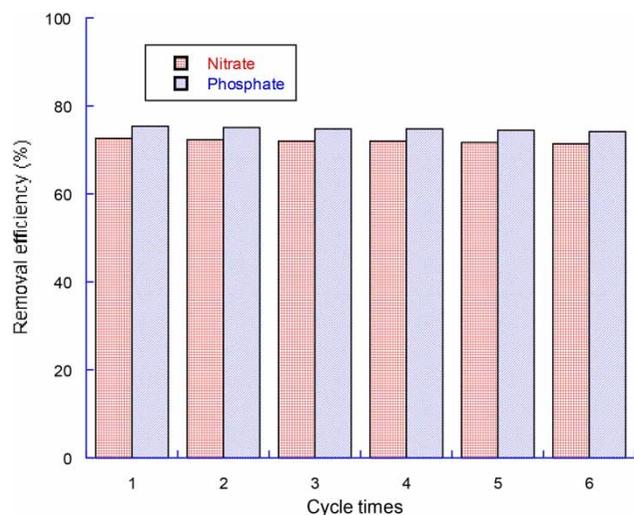
Figure 15 | Reusability of the CTS:PVA (1:2) composite for the removal of nitrate and phosphate ions.

CONCLUSIONS

In this study, crab shell chitosan and a CTS/PVA composite were successfully synthesized. With 90% DD, as-synthesized chitosan did not contain inorganic mineral, as confirmed by FTIR spectroscopy, EDX analysis and titration. As-synthesized chitosan also exhibited better antibacterial properties against *S. aureus* than *E. coli*. Besides, when thin films were formed, these chitosan molecules exhibited small uniform particles with a size of 50–70 nm. The optimal conditions for the preparation of crab shell chitosan were derived by an optimized method that utilized the Box–Behnken design, such as an HCl concentration of 1.62 M, a protein removal time of 95.64 min and a deacetylation time of 177.3 min while simultaneously maintaining other conditions constant, as outlined in previous sections. The SEM image revealed that the CTS/PVA (1:2) composite was also successfully prepared with a width of 100–200 nm and a thickness of 20–30 nm. Among the investigated adsorbents, crab shell chitosan and the CTS/PVA (1:2) composite exhibited the highest adsorption efficiency for nitrate and phosphate ions. However, their ability to adsorb phosphate ions was better than that to adsorb nitrate ions, and the adsorption capacity of the CTS/PVA (1:2) composite was better than that of crab shell chitosan. The adsorption of these materials for phosphate and nitrate

ions fitted well with the Langmuir isotherm adsorption model and pseudo-second-order adsorption kinetics. The adsorption efficiencies of composite material for nitrate and phosphate ions after six adsorption–desorption cycles were nearly unchanged. These results demonstrate potential for the use of the CTS: PVA (1:2) composite to adsorb nitrate and phosphate for wastewater treatment.

DATA AVAILABILITY STATEMENT

All relevant data are included in the paper or its Supplementary Information.

REFERENCES

Bhatnagar, A. & Sillanpää, M. 2011 A review of emerging adsorbents for nitrate removal from water. *Chemical Engineering Journal* **168** (2), 493–504. http://dx.doi.org/10.1016/j.cej.2011.01.103.

Bonilla, J., Fortunati, E., Atarés, L., Chiralt, A. & Kenny, J. M. 2014 Physical, structural and antimicrobial properties of poly vinyl alcohol-chitosan biodegradable films. *Food Hydrocolloids* **35**, 463–470. http://dx.doi.org/10.1016/j.foodhyd.2013.07.002.

Bui, M. H., Pham, T. L. & Dao, T. S. 2017 Prediction of cyanobacterial blooms in the Dau Tieng Reservoir using an artificial neural network. *Marine and Freshwater Research* **68** (11), 2070–2080.

Dai, L., Wang, Y., Li, Z., Wang, X., Duan, C., Zhao, W., Xiong, C., Nie, S., Xu, Y. & Ni, Y. 2020 A multifunctional self-crosslinked chitosan/cationic guar gum composite hydrogel and its versatile uses in phosphate-containing water treatment and energy storage. *Carbohydrate Polymers* **244**, 116472. https://doi.org/10.1016/j.carbpol.2020.116472.

Das, L., Das, P., Bhowal, A. & Bhattachariee, C. 2020 Synthesis of hybrid hydrogel nano-polymer composite using graphene oxide, chitosan and PVA and its application in waste water treatment. *Environmental Technology and Innovation* **18**, 100664. https://doi.org/10.1016/j.eti.2020.100664.

Dodds, W. K. & Smith, V. H. 2016 Nitrogen, phosphorus, and eutrophication in streams. *Inland Waters* **6** (2), 155–164.

Ghadiri, S. K., Nasseri, S., Nabizadeh, R., Khoobi, M., Nazmara, S. & Mahvi, A. H. 2017 Adsorption of nitrate onto anionic bio-graphene nanosheet from aqueous solutions: isotherm and kinetic study. *Journal of Molecular Liquids* **242**, 1111–1117. http://dx.doi.org/10.1016/j.molliq.2017.06.122.

He, H., Huang, Y., Yan, M., Xie, Y. & Li, Y. 2020 Synergistic effect of electrostatic adsorption and ion exchange for efficient removal of nitrate. *Colloids and Surfaces A: Physicochemical and Engineering Aspects* **584**, 123973. Available from:

http://www.sciencedirect.com/science/article/pii/S092777571930963X.

Huang, L., Bi, S., Pang, J., Sun, M., Feng, C. & Chen, X. 2020 Preparation and characterization of chitosan from crab shell (*Portunus trituberculatus*) by NaOH/urea solution freeze-thaw pretreatment procedure. *International Journal of Biological Macromolecules* **147**, 931–936. https://doi.org/10.1016/j.ijbiomac.2019.10.059.

Li, J., Dong, S., Wang, Y., Dou, X. & Hao, H. 2020a Nitrate removal from aqueous solutions by magnetic cationic hydrogel: effect of electrostatic adsorption and mechanism. *Journal of Environmental Sciences (China)* **91**, 177–188. https://doi.org/10.1016/j.jes.2020.01.029.

Li, J., Li, B., Huang, H., Zhao, N., Zhang, M. & Cao, L. 2020b Investigation into lanthanum-coated biochar obtained from urban dewatered sewage sludge for enhanced phosphate adsorption. *Science of the Total Environment* **714**, 136839. https://doi.org/10.1016/j.scitotenv.2020.136839.

Muxika, A., Etxabide, A., Uranga, J., Guerrero, P. & de la Caba, K. 2017 Chitosan as a bioactive polymer: processing, properties and applications. *International Journal of Biological Macromolecules* **105**, 1358–1368. https://doi.org/10.1016/j.ijbiomac.2017.07.087.

Pérez-Álvarez, L., Ruiz-Rubio, L. & Vilas-Vilela, J. L. 2018 Determining the deacetylation degree of chitosan: opportunities to learn instrumental techniques. *Journal of Chemical Education* **95** (6), 1022–1028.

Pham, T. L. & Bui, M. H. 2020 Removal of nutrients from fertilizer plant wastewater using *Scenedesmus* sp.: formation of bioflocculation and enhancement of removal efficiency. *Journal of Chemistry* **809292**, 1–9.

Quesada, H. B., de Araújo, T. P., Vareschini, D. T., de Barros, M. A. S. D., Gomes, R. G. & Bergamasco, R. 2020 Chitosan, alginate and other macromolecules as activated carbon immobilizing agents: a review on composite adsorbents for the removal of water contaminants. *International Journal of Biological Macromolecules* **164**, 2535–2549. https://doi.org/10.1016/j.ijbiomac.2020.08.118.

Rahmi, C. N. A., Husnina, A. N., Trismiarni, M. E., Putri, M. D. C., Sudistya, D., Julianto, T. S. & Salmahaminati, S. 2017 Synthesis of chitosan from the crab shell with encapsulation method. *Journal of Engineering and Applied Sciences* **12** (18), 4725–4729.

Rajeswari, A., Amalraj, A. & Pius, A. 2015 *Removal of Phosphate Using Chitosan-Polymer Composites*. Elsevier B.V., Amsterdam, The Netherlands. http://dx.doi.org/10.1016/j.jece.2015.08.022.

Rajeswari, A., Amalraj, A. & Pius, A. 2016 Adsorption studies for the removal of nitrate using chitosan/PEG and chitosan/PVA polymer composites. *Journal of Water Process Engineering* **9**, 123–134. http://dx.doi.org/10.1016/j.jwpe.2015.12.002.

Rao, J. S. & Kumar, B. 2012 *3D Blade Root Shape Optimization*. Woodhead Publishing Limited, Cambridge, UK. http://dx.doi.org/10.1533/9780857094537.4.173.

Sarbon, N. M., Sandanamsamy, S., Kamaruzaman, S. F. S. & Ahmad, F. 2014 Chitosan extracted from mud crab (*Scylla olivicea*) shells: physicochemical and antioxidant properties. *Journal of Food Science and Technology* **52** (7), 4266–4275.

dos Santos, Z. M., Caroni, A. L. P. F., Pereira, M. R., da Silva, D. R. & Fonseca, J. L. C. 2009 Determination of deacetylation degree of chitosan: a comparison between conductometric titration and CHN elemental analysis. *Carbohydrate Research* **344** (18), 2591–2595. http://dx.doi.org/10.1016/j.carres.2009.08.030.

Shavandi, A., Bekhit, A. A., Bekhit, A. E. D. A., Sun, Z. & Ali, M. A. 2015 Preparation and characterisation of irradiated crab chitosan and New Zealand Arrow squid pen chitosan. *Materials Chemistry and Physics* **167**, 295–302. http://dx.doi.org/10.1016/j.matchemphys.2015.10.047.

Srinivasan, H., Kanayairam, V. & Ravichandran, R. 2018 Chitin and chitosan preparation from shrimp shells *Penaeus monodon* and its human ovarian cancer cell line, PA-1. *International Journal of Biological Macromolecules* **107** (PartA), 662–667. http://dx.doi.org/10.1016/j.ijbiomac.2017.09.035.

van Puijenbroek, P. J. T. M., Beusen, A. H. W. & Bouwman, A. F. 2019 Global nitrogen and phosphorus in urban waste water based on the shared socio-economic pathways. *Journal of Environmental Management* **231**, 446–456. https://doi.org/10.1016/j.jenvman.2018.10.048.

Yang, Q., Gong, L., Huang, L., Xie, Q., Zhong, Y. & Chen, N. 2020 Adsorption of As(V) from aqueous solution on chitosan-modified diatomite. *International Journal of Environmental Research and Public Health* **17** (2), 1–15.

Yin, Q., Ren, H., Wang, R. & Zhao, Z. 2018 Evaluation of nitrate and phosphate adsorption on Al-modified biochar: influence of Al content. *Science of the Total Environment* **631–632**, 895–903.

Yuan, Y., Chesnutt, B. M., Haggard, W. O. & Bumgardner, J. D. 2011 Deacetylation of chitosan: material characterization and in vitro evaluation via albumin adsorption and pre-osteoblastic cell cultures. *Materials* **4** (8), 1399–1416.

Zhang, B., Chen, N., Feng, C. & Zhang, Z. 2018 Adsorption for phosphate by crosslinked/non-crosslinked-chitosan-Fe(III) complex sorbents: characteristic and mechanism. *Chemical Engineering Journal* **353** (July), 361–372. https://doi.org/10.1016/j.cej.2018.07.092.

Zheng, Q., Yang, L., Song, D., Zhang, S., Wu, H., Li, S. & Wang, X. 2020 High adsorption capacity of Mg–Al-modified biochar for phosphate and its potential for phosphate interception in soil. *Chemosphere* **259**, 127469. https://doi.org/10.1016/j.chemosphere.2020.127469.